JOURNAL OF SOLID STATE CHEMISTRY **138,** 238–244 (1998)
ARTICLE NO. SC987775

Crystal Chemistry of Cation Order–Disorder in Pseudobrookite-Type $MgTi_2O_5$

Hexiong Yang and Robert M. Hazen

Geophysical Laboratory and Center for High Pressure Research, Carnegie Institution of Washington, 5251 Broad Branch Road, NW, Washington, DC 20015–1305

Received November 3, 1997; in revised form January 27, 1998; accepted January 28, 1998

Effects of cation order–disorder on the pseudobrookite-type $MgTi_2O_5$ structure have been studied with single-crystal X-ray diffraction on five synthetic crystals (labeled P600, P700, P800, P1000, and P1400) annealed at 600, 700, 800, 1000, and 1400°C, respectively. The disorder parameters (X = Ti in the $M1$ site) determined for five samples range from 0.070(5) to 0.485(5). Unit-cell dimensions a and c increase with X, whereas b decreases. The decrease in b with increasing cation disorder results primarily from the marked reduction in the O3–O3 distance within the $M1$ octahedron, whereas the variation of a and c is controlled by the size of the $M2$ octahedron. From P600 to P1400, the mean $M1$–O length shortens by 2.35%; in contrast, the mean $M2$–O distance lengthens by 1.16%. As a consequence, the $M1$ and $M2$ sites have a nearly identical octahedral volume in P1400. With increasing cation disorder, the degree of distortion of the $M1$ octahedron is reduced significantly, while that of $M2$ remains essentially unchanged. Cation disorder is also accompanied by straightening of the bands consisting of the $M1$ and $M2$ octahedra. There is a close correlation between atomic isotropic displacement factors (B_{iso}) and cation order–disorder: B_{iso} factors of all atoms in more disordered samples are larger than those in less disordered ones. © 1998 Academic Press

INTRODUCTION

$MgTi_2O_5$, the end member of the pseudobrookite-type $(Mg,Fe)Ti_2O_5$ (armalcolite) solid solution, is of geological interest because of its occurrence in many volcanic and metamorphic rocks. It is also an important constituent of refractory ceramics and magnetic materials and exhibits unusually large thermal expansion anisotropy (1). From the crystal-chemistry point of view, of particular interest is the wide range of the nonconvergent cation order–disorder between two crystallographically distinct octahedral sites in the $MgTi_2O_5$ structure, which has been regarded to be responsible for its high-temperature stabilization (2) and notable structural changes (3–5). Furthermore, Hazen and Yang (6) demonstrated that the cation disorder can increase the compressibility of $MgTi_2O_5$ by as much as 6% and suggested that cation disorder, in addition to composition and structure, can also significantly affect the elasticity of crystalline phases.

$MgTi_2O_5$ possesses the pseudobrookite structure with space group *Bbmm* and its structure was first refined by Lind and Housley (7). All cations occupy two nonequivalent, highly distorted octahedral sites, $M1$ and $M2$, with $M1$ larger and more distorted than $M2$. The polyhedral linkage of $M1$ and $M2$ is characterized by complex edge sharing. On the one hand, $M1$ and $M2$ share edges to form bands extending in the b direction (Fig. 1); on the other, each $M2$ shares four octahedral edges with others to form $M2$ octahedral layers parallel to (010); these layers are linked together along b by $M1$ through edge sharing as well (6). Previous studies on armalcolite ($Fe_{0.5}Mg_{0.5}Ti_2O_5$) show that $M1$ is preferentially occupied by Fe and Mg, and $M2$ by Ti, and that the cation distribution in these compounds is temperature dependent: samples quenched from higher temperatures are substantially more disordered than those quenched from lower temperatures (3–5, 7–11). Wechsler and Navrotsky (4) further found that the unit-cell parameters of $MgTi_2O_5$ depend strongly on the cation ordering state or quenching temperature: a, c, and V increase with increasing quenching temperature, whereas b decreases. They also reported that this dependence is markedly sigmoid, with little change at temperatures below 700°C or above 1100°C. Brown and Navrotsky (12) developed an empirical structural model for determining the degree of disorder in $MgTi_2O_5$ from unit-cell parameters. However, due to the lack of single-crystal X-ray diffraction data, this model was calibrated only on the basis of structural data and site occupancies on armalcolite reported by Smyth (8) and Wechsler (3). Despite the sophistication of the model proposed by Brown and Navrotsky (12), caution should be exercised when it is applied to the end members, because of the difficulty in accurately determining site occupancies of three cations (Fe, Mg, and Ti) between two sites in $Fe_{0.5}Mg_{0.5}Ti_2O_5$ (3, 7, 8, 11). We have undertaken a single-crystal X-ray diffraction study on five synthetic $MgTi_2O_5$ crystals annealed at 600, 700, 800, 1000, and 1400°C to

0022-4596/98 $25.00
Copyright © 1998 by Academic Press
All rights of reproduction in any form reserved.

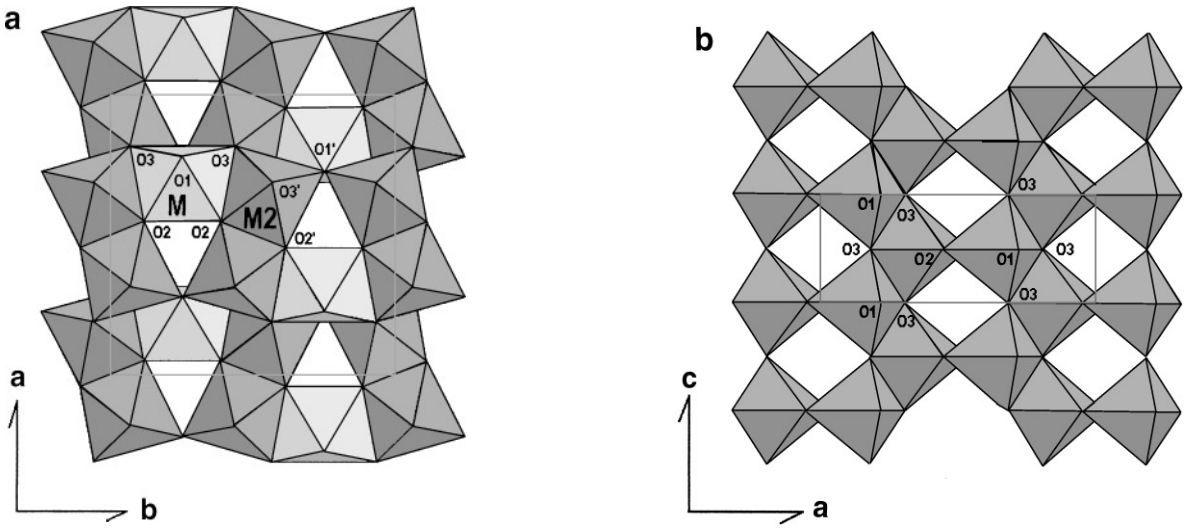

FIG. 1. Crystal structure of pseudobrookite-type $MgTi_2O_5$: (a) viewed along *c*, showing the bands of the *M*1 and *M*2 octahedra, and (b) viewed along *b*, showing the edge-shared *M*2 octahedral layer.

characterize variations of the unit-cell parameters and crystal structure of $MgTi_2O_5$ with cation order–disorder. The results reported in this paper are a part of our systematic investigations into the pressure effects on atomic order–disorder in crystalline phases.

EXPERIMENTAL

Sample Preparation

All samples used in this study were synthesized by the flux method. Dried reagent-grade MgO and TiO_2 were weighed in stoichiometric proportions and ground manually under methanol in an agate mortar. The mixture in a Pt crucible was first heated in air in a vertical tube furnace at 1400°C for 48 h. Following another grinding with K_2WO_4 added as flux (the weight ratio of $MgTi_2O_5 : K_2WO_4$ was 1 : 1), the powder was again heated at 1400°C for 48 h and cooled to 1200°C in about 6 h. After being held at 1200°C for 5 days, the sample was quenched to room temperature. Optical and X-ray diffraction examination of the final product revealed the presence of two phases: more than 99% of white and transparent $MgTi_2O_5$ crystals plus some yellowish crystals with the hollandite structure. Most $MgTi_2O_5$ crystals are elongated along the *c* axis; the longest dimension of the largest crystal is greater than 1 mm. The chemical composition was analyzed with an electron microprobe on four crystals; within the experimental uncertainties, no W or K was detected and all crystals were found to have a nearly ideal chemical formula: $Mg_{0.995\pm0.006}Ti_{2.005\pm0.005}O_5$. For simplicity, we assumed stoichiometry for all final structure refinements.

Quenching experiments were performed in a vertical tube furnace at 600, 700, 800, 1000, and 1400°C. In the following, we use the abbreviations P600, P700, P800, P1000, and P1400 for the samples quenched from 600, 700, 800, 1000, and 1400°C, respectively. Each sample was enclosed in a Pt-foil envelope and suspended in air in the furnace by a Pt wire. The variation in temperature, measured by a thermocouple adjacent to the sample, was within ± 1°C. The heating duration of each sample is given in Table 1. Quenching was achieved by cutting (for P600, P700, and P800) or melting (for P1000 and P1400) Pt wires and dropping the samples into mercury.

X-Ray Diffraction Data Measurements

A single crystal from each quenched sample was selected on the basis of optical examination and precession photographs and polished to the desired size ($\sim 0.10 \times 0.10 \times 0.04$ mm) suitable for high-pressure X-ray diffraction study. A Picker four-circle diffractometer equipped with a Mo X-ray tube (β-filtered) was used for all X-ray diffraction data measurements. Unit-cell parameters were determined by fitting the positions of 16 reflections with $20° < 2\theta < 35°$ following the procedure of King and Finger (13) (Table 1).

For all crystals, X-ray diffraction intensity data from one quadrant of reciprocal space with $0° \leq 2\theta \leq 60°$ were collected on the basis of the *B*-centered lattice using ω scans of 1° width in step increments of 0.025° and 2-s/step counting time. Two standard reflections were checked every 5 h; no significant or systematic variations in intensities of the standard reflections were observed. Digitized step data were integrated by the method of Lehmann and Larsen (14), with background manually reset when necessary. Corrections were made for Lorentz and polarization effects and for X-ray absorption by the crystal. Reflections having

TABLE 1
Crystal Data and Other Relevant Information on Karrooite ($MgTi_2O_5$) Annealed at Various Temperatures

Sample	P600	P700	P800	P1000	P1400
Quenching T (°C)	600	700	800	1000	1400
Heating time (h)	1008	840	504	168	5
a (Å)	9.7115(5)	9.7264(3)	9.7378(3)	9.7461(6)	9.7597(4)
b (Å)	10.0189(3)	10.0092(3)	9.9976(2)	9.9875(4)	9.9789(4)
c (Å)	3.7362(2)	3.7409(2)	3.7440(2)	3.7464(4)	3.7478(3)
V (Å^3)	363.52(3)	364.19(3)	364.50(2)	364.67(4)	365.00(3)
ρ (g/cm^3)	3.656	3.649	3.646	3.644	3.641
μ (cm^{-1})	44.127	44.045	44.008	43.987	43.948
Reflections $> 3\sigma(I)$	306	301	303	303	311
R_{merge}	0.020	0.011	0.014	0.021	0.013
R_w	0.022	0.019	0.029	0.026	0.027
R	0.020	0.017	0.027	0.023	0.023
X^a	0.070(5)	0.203(3)	0.306(5)	0.404(5)	0.485(5)

[a] Disorder parameter. Ti in $M1 = X$; Mg in $M1 = 1 - X$; Ti in $M2 = 1 - X/2$; Mg in $M2 = X/2$.

TABLE 2
Atomic Positional and Displacement Parameters of $MgTi_2O_5$ Annealed at Various Temperatures

	600°C	700°C	800°C	1000°C	1400°C
*M*1					
x	0.80512(7)	0.80619(5)	0.80688(6)	0.80759(7)	0.80855(6)
β_{11}	0.0014(1)	0.0015(0)	0.0016(1)	0.0015(1)	0.0015(1)
β_{22}	0.0013(1)	0.0013(1)	0.0012(1)	0.0015(1)	0.0015(1)
β_{33}	0.0092(6)	0.0113(3)	0.0108(5)	0.0097(6)	0.0115(6)
B	0.53(3)	0.59(2)	0.55(2)	0.56(3)	0.60(3)
*M*2					
x	0.13344(3)	0.13418(2)	0.13471(3)	0.13523(4)	0.13571(3)
y	0.43326(3)	0.43449(2)	0.43536(3)	0.43614(4)	0.43679(4)
β_{11}	0.0012(1)	0.0012(1)	0.0014(1)	0.0011(1)	0.0014(1)
β_{22}	0.0011(1)	0.0014(1)	0.0012(1)	0.0015(1)	0.0016(1)
β_{33}	0.0067(3)	0.0092(2)	0.0087(3)	0.0078(4)	0.0102(4)
β_{12}	0.0000(1)	−0.0001(1)	−0.0001(1)	−0.0001(1)	−0.0001(1)
B	0.43(2)	0.51(1)	0.50(2)	0.49(2)	0.58(2)
O1					
x	0.21924(18)	0.22355(13)	0.22702(20)	0.23094(23)	0.23445(21)
β_{11}	0.0024(1)	0.0028(1)	0.0031(2)	0.0029(2)	0.0030(2)
β_{22}	0.0010(1)	0.0014(1)	0.0014(2)	0.0019(2)	0.0021(2)
β_{33}	0.0105(10)	0.0149(7)	0.0152(11)	0.0149(14)	0.0176(13)
B	0.62(4)	0.82(3)	0.86(4)	0.89(5)	0.99(4)
O2					
x	0.04572(11)	0.04621(9)	0.04651(12)	0.04670(15)	0.04705(13)
y	0.88643(12)	0.88567(9)	0.88518(13)	0.88450(17)	0.88376(16)
β_{11}	0.0014(1)	0.0018(1)	0.0021(1)	0.0018(1)	0.0024(1)
β_{22}	0.0014(1)	0.0014(1)	0.0014(1)	0.0017(1)	0.0018(1)
β_{33}	0.0197(8)	0.0231(6)	0.0216(9)	0.0218(11)	0.0240(10)
β_{12}	0.0000(1)	−0.0002(1)	−0.0001(1)	−0.0001(1)	0.0000(1)
B	0.73(3)	0.85(2)	0.86(3)	0.87(3)	0.98(3)
O3					
x	0.31371(13)	0.31302(9)	0.31239(13)	0.31197(16)	0.31135(15)
y	0.93772(11)	0.93552(8)	0.93366(13)	0.93236(16)	0.93042(15)
β_{11}	0.0017(1)	0.0020(1)	0.0023(1)	0.0021(2)	0.0025(1)
β_{22}	0.0018(1)	0.0020(1)	0.0017(1)	0.0023(1)	0.0022(1)
β_{33}	0.0069(7)	0.0107(5)	0.0109(8)	0.0103(11)	0.0128(10)
β_{12}	0.0000(1)	−0.0001(1)	−0.0001(1)	−0.0001(1)	−0.0001(1)
B	0.59(3)	0.71(2)	0.72(3)	0.77(4)	0.86(3)

Note. The following constraints apply to some atomic positional coordinates: $y = 1/4$ for $M1$ and O1; $z = 0$ for all atoms. The following constraints apply to some atomic anisotropic displacement parameters: $\beta_{12} = \beta_{13} = \beta_{23} = 0$ for $M1$ and O1; $\beta_{13} = \beta_{23} = 0$ for $M2$, O2, and O3.

$I > 2\sigma(I)$ were considered as observed and included in the refinement, where $\sigma(I)$ is the standard deviation determined from the counting statistics. Symmetry equivalent reflections for each data set were averaged in Laue group *mmm*.

The initial structural model of $MgTi_2O_5$ was taken from Wechsler and Von Dreele (5). Least-squares refinements were carried out using an updated version of RFINE4 (15) in space group *Bbmm*. Neutral atomic scattering factors, including anomalous dispersion correction for Mg, Ti, and O, were taken from Ibers and Hamilton (16). Weighting schemes were based on $w = [\sigma^2(F) + (pF)^2]^{-1}$, where p is adjusted to ensure that the errors were normally distributed through probability plot analysis (16). The Mg and Ti occupancies between the $M1$ and $M2$ sites were allowed to vary during refinements with the bulk composition constrained to the ideal chemical formula. All refinements converged smoothly after four to six cycles. Type II isotropic extinction corrections (17) were applied in the refinements. Atomic positional coordinates and displacement parameters are listed in Table 2. Selected interatomic distances, along with polyhedral distortion indices, and angles are presented in Tables 3 and 4, respectively.

RESULTS AND DISCUSSION

Unit-Cell Parameters as a Function of Cation Disordering

Unit-cell parameters of $MgTi_2O_5$ as a function of quenching temperature are plotted in Fig. 2. Data determined by Brown and Navrotsky (12) are also included for comparison. Within experimental errors, our data between 700 and 1000°C agree with those reported previously, but the data at 600 and 1400°C deviate from the trend defined by previous data. Specifically, the unit-cell volume of P1400 is larger than any other volume reported from quenching experiments, whereas that of P600 is smaller. Thus, our data point to a significantly larger volume of disordering, ΔV_{dis}, than previously suggested [ΔV_{dis} is the unit-cell volume difference between the most disordered and ordered samples (18)]. It should be pointed out that to achieve the largest ΔV_{dis} value, we also annealed a sample at 1500°C and one at 500°C. However, the unit-cell dimensions of the sample annealed at 1500°C for 5 h do not differ significantly from those of P1400, suggesting the rapid kinetics of cation fractionation at this temperature such that the cation ordering

TABLE 3
Interatomic Distances (Å) and Octahedral Distortion Indices of $MgTi_2O_5$ Annealed at Various Temperatures

	600°C	700°C	800°C	1000°C	1400°C
*M*1–O1 [×2]	2.046(1)	2.036(1)	2.027(1)	2.017(1)	2.009(1)
*M*1–O2 [×2]	1.992(1)	1.976(1)	1.966(1)	1.955(2)	1.941(2)
*M*1–O3 [×2]	2.207(1)	2.189(1)	2.173(1)	2.162(2)	2.147(2)
Average	2.081	2.067	2.055	2.045	2.032
O1–O2	3.251(2)	3.218(1)	3.193(2)	3.164(2)	3.137(2)
O1–O3	2.670(1)	2.660(1)	2.650(1)	2.646(1)	2.637(1)
O2–O2′	2.734(2)	2.716(2)	2.703(3)	2.687(3)	2.670(3)
O2–O3	2.653(2)	2.643(1)	2.634(2)	2.629(2)	2.621(2)
O3–O3′	3.761(2)	3.714(1)	3.672(3)	3.643(3)	3.601(3)
OV[a]	10.525(5)	10.403(5)	10.303(5)	10.220(10)	10.104(9)
OQE	1.0947(2)	1.0881(1)	1.0829(2)	1.0775(3)	1.0727(3)
OAV	255.7(3)	240.2(1)	228.1(2)	214.9(3)	203.1(3)
*M*2–O1 [×1]	2.016(1)	2.041(1)	2.060(1)	2.080(1)	2.098(1)
*M*2–O2′[×1]	1.997(1)	1.993(1)	1.989(1)	1.988(2)	1.989(2)
*M*2–O2 [×1]	1.802(1)	1.821(1)	1.835(1)	1.847(2)	1.860(1)
*M*2–O3 [×1]	2.176(1)	2.172(1)	2.170(1)	2.166(2)	2.167(2)
*M*2–O3′[×2]	1.938(1)	1.940(1)	1.942(1)	1.943(1)	1.945(1)
Average	1.978	1.985	1.989	1.995	2.001
O1–O2′	2.914(2)	2.954(1)	2.987(2)	3.021(3)	3.054(2)
O1–O3	3.260(1)	3.266(1)	3.270(1)	3.269(2)	3.276(2)
O1–O3′	2.670(1)	2.660(1)	2.650(1)	2.646(1)	2.637(1)
O2–O2′	2.443(2)	2.459(1)	2.468(3)	2.480(3)	2.495(3)
O2′–O3′	2.972(1)	2.982(1)	2.989(1)	2.995(2)	3.003(2)
O2–O3	2.653(2)	2.643(1)	2.634(2)	2.629(2)	2.621(2)
O2–O3′	2.908(1)	2.929(1)	2.945(1)	2.958(2)	2.977(2)
O3–O3′	2.565(2)	2.582(1)	2.596(2)	2.606(2)	2.622(2)
OV	9.767(5)	9.867(4)	9.940(5)	10.018(9)	10.100(8)
OQE	1.0406(1)	1.0400(1)	1.0399(1)	1.0397(2)	1.0403(2)
OAV	124.7(1)	123.6(1)	124.1(1)	124.0(3)	126.2(3)

[a] OV, octahedral volume; OQE, octahedral quadratic elongation; OAV, octahedral angle variance (19).

TABLE 4
Interatomic Angles in $MgTi_2O_5$ Annealed at Various Temperatures

	600°C	700°C	800°C	1000°C	1400°C
O1–*M*1–O2	107.25(3)	106.67(2)	106.18(4)	105.61(4)	105.15(4)
O1–*M*1–O3	77.69(3)	77.93(2)	78.17(3)	78.48(4)	78.68(3)
O2–*M*1–O2	86.68(7)	86.81(5)	86.86(8)	86.82(9)	86.89(9)
O2–*M*1–O3	78.19(5)	78.57(3)	78.88(5)	79.20(6)	79.58(6)
O3–*M*1–O3	116.93(7)	116.04(5)	115.37(7)	114.78(9)	113.96(8)
O1–*M*2–O2	99.32(6)	99.65(4)	100.01(6)	100.43(8)	100.81(7)
O1–*M*2–O3	102.03(6)	101.59(4)	101.24(6)	100.68(7)	100.37(6)
O1–*M*2–O3	84.93(4)	83.80(3)	82.90(4)	82.18(5)	81.31(5)
O2–*M*2–O2	79.84(6)	80.14(4)	80.29(6)	80.50(8)	80.73(7)
O2–*M*2–O3	105.17(4)	104.86(3)	104.64(4)	104.41(5)	104.21(4)
O2–*M*2–O3	78.81(5)	78.63(3)	78.46(5)	78.39(6)	78.09(6)
O2–*M*2–O3	95.29(4)	96.25(3)	97.03(4)	97.61(5)	98.34(5)
O3–*M*2–O3	76.89(4)	77.57(3)	78.10(4)	78.53(5)	79.04(4)
O3–O1–O3	147.31(7)	149.05(5)	150.55(8)	152.04(9)	153.51(9)
O3–O3–O1	163.66(4)	164.55(3)	165.27(4)	166.02(5)	166.76(4)

state above 1400°C may not be quenchable. The unit-cell dimensions of the sample annealed at 500°C for 60 days, on the other hand, are similar to those of P1000, indicating a sluggish Mg–Ti order–disorder process at this temperature. This observation is different from that made by Wechsler and Navrotsky (4), who reported that the cation distribution may equilibrate at 500°C on a time scale of weeks.

In Fig. 3, we plotted the cation disorder parameter (X = Ti in $M1$) versus quenching temperature; the data used in the figure are from this study and Brown and Navrotsky (12). It is apparent that our data exhibit a stronger dependence of X on quenching temperature. By combining Figs. 1 and 2, we found that the unit-cell dimensions of a and b vary linearly with X, whereas c and thus V vary nonlinearly with a negative curvature:

$$a\ (\text{Å}) = 9.7031 + 0.1117X, \qquad \gamma^2 = 0.989,$$

$$b\ (\text{Å}) = 10.0262 - 0.0960X, \qquad \gamma^2 = 0.999,$$

$$c\ (\text{Å}) = 3.7329 + 0.0487X - 0.0376X^2, \qquad \gamma^2 = 0.999,$$

$$V\ (\text{Å}^3) = 363.17 + 4.72X - 2.36X^2, \qquad \gamma^2 = 0.993,$$

where γ is the correlation coefficient. From the above equations, the unit-cell dimensions estimated for fully ordered $MgTi_2O_5$ are $a = 9.7031$, $b = 10.0262$, $c = 3.7329$ Å, and $V = 363.17$ Å^3, and those for fully disordered $MgTi_2O_5$ are $a = 9.7785$, $b = 9.9638$, $c = 3.7495$ Å, and $V = 365.32$ Å^3. The nonlinear dependence of V on X indicates the nonideality of ΔV_{dis}, which could be a reflection of the nonideal mixing of Mg/Ti at both $M1$ and $M2$ sites (see below).

Brown and Narvotsky (12) suggested the c dimension is the most useful lattice parameter for calculating X among all unit-cell parameters. However, the equations we obtained above indicate that the a and b dimensions are not only a linear function of X, but also more sensitive than the c dimension in response to the change in X. Accordingly, the a and b dimensions should serve better for estimating the disorder parameter in $MgTi_2O_5$.

Structural Changes with Mg–Ti Order–Disorder

One of the most significant effects of cation order–disorder on the $MgTi_2O_5$ structure is the change in the M–O bond lengths. As the disorder parameter changes from 0.070 in P600 to 0.485 in P1400, the average $M1$–O bond distance shortens by 2.35%; in contrast, the average $M2$–O bond

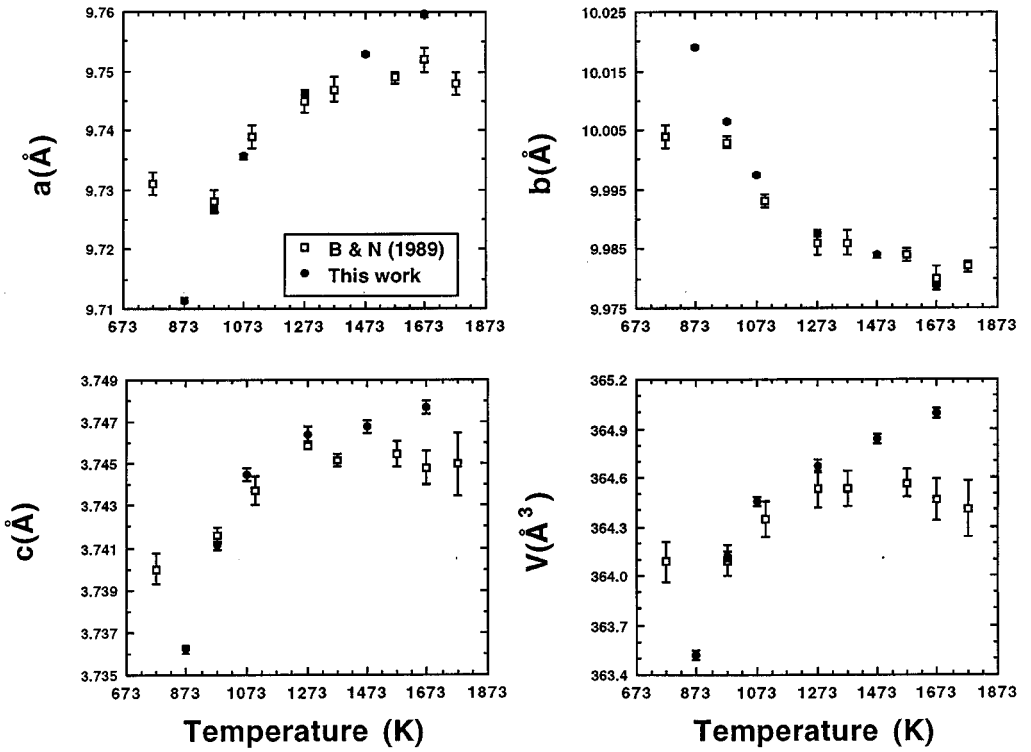

FIG. 2. Unit-cell parameters of $MgTi_2O_5$ as a function of quenching temperature.

distance lengthens by 1.16%. As a consequence, the difference between the $M1$ and $M2$ octahedral volumes decreases, such that the two octahedra have nearly identical volumes in P1400 ($\sim$10.10 Å^3). In detail, all individual $M1$–O bond lengths decrease from P600 to P1400, with the $M1$–O3 distance shortening most (2.8%) and the $M1$–O1 distance least (1.7%). Because the $M1$–O3 bond length shows the largest deviation from the mean $M1$–O distance within the $M1$ octahedron, its greatest reduction gives rise to a decrease in $M1$ octahedral distortion: the octahedral quadratic elongation (OQE) (19) changes from 1.0947(2) in P600 to 1.0727(3) in P1400. Within the $M2$ octahedron, however, while the respective $M2$–O1 and $M2$–O2′ bond lengths increase by as much as 4.1 and 3.2% from P600 to P1400, the $M2$–O2 and $M2$–O3 bond distances decrease by $\sim$0.4%. Such contrasting behavior of individual $M2$–O bonds results in an essentially unchanged OQE value for $M2$. The slight shortening of the $M2$–O2 and $M2$–O3 bond lengths with the substitution of larger Mg^{2+} (r = 0.78 Å) for smaller Ti^{4+} (r = 0.50Å) (20) in the $M2$ site is related to the change in the $M1$–$M2$ separation, which decreases from 3.229 Å in P600 to 3.172 Å in P1400. To reduce the cation-cation repulsion between $M1$ and $M2$ in more disordered samples, all lengths of O–O edges shared by the $M1$ and $M2$ octahedra (O1–O3′ and O2–O3) become shorter (Table 3). In contrast, all lengths of O–O edges shared by two $M2$ octahedra (O2–O2′ and O3–O3′) become longer in more disordered samples, owing to the increase in the $M2$–$M2$ separation from 2.916 Å in P600 to 2.934 Å in P1400.

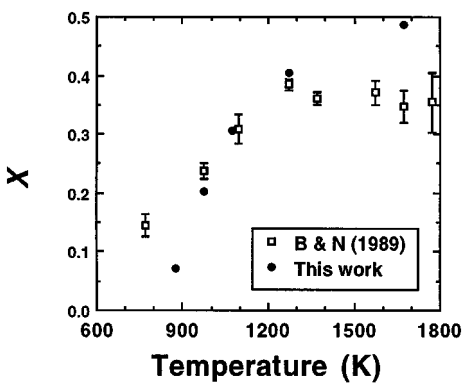

FIG. 3. Variation of the cation disorder parameter (X) with quenching temperature. Open squares are the data of Brown and Navrotsky (12).

Wechsler and Von Dreele (5) refined structures of five crystals in the MgO–TiO_2 system, which include one $MgTiO_3$, two Mg_2TiO_4, and two $MgTi_2O_5$ phases. In the plot of the mean M–O bond lengths versus the Ti fraction in the octahedral sites, they found a small negative deviation from Vegard's law for mixing Mg and Ti on these sites and concluded that this nonideality appears to have little effect

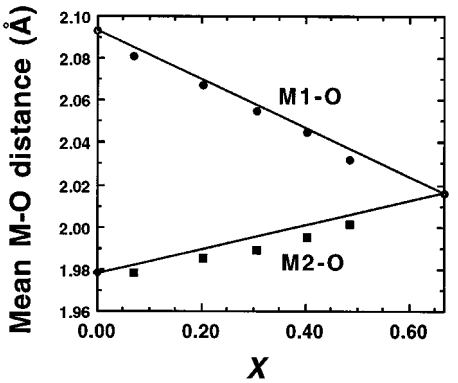

FIG. 4. Mean M–O bond lengths for octahedral sites in $MgTi_2O_5$ as a function of cation disorder parameter (X). Straight lines were drawn between completely ordered and disordered phases based on the ionic radii of Shannon and Prewitt (20).

on the temperature dependence of the disordering, but might give rise to a slight tendency to greater disorder in these phases at higher pressures. A plot of our data for $MgTi_2O_5$ crystals with various ordering states (Fig. 4) displays a result similar to that observed by Wechsler and Von Dreele (5). It also shows that the mean $M2$–O bond length appears to exhibit slightly greater nonideality than the mean $M1$–O distance.

Associated with the variations of M–O distances as a function of cation disorder are the pronounced changes in interatomic bond angles within and between the two different octahedra. Compared with the $M2$ octahedron, which displays little change in its angular distortion index, the octahedral angle variance (OAV) (19), the OAV value for $M1$ decreases appreciably from 255.7(3) to 203.1(3), a 21% reduction. This change is due primarily to the fact that the angular deviations of all O–$M1$–O angles from the ideal value of 90° decrease with increasing cation disorder. Among all O–$M1$–O angles, the largest O3–$M1$–O3 angle changes most, from 116.9(1)° in P600 to 114.0(1)° in P1400. Coupled with the marked decrease in the O3–$M1$–O3 angle is a 4.3% shortening of the O3–O3 distance, the greatest decrease of all O–O distances within the $M1$ octahedron. The essentially unchanged OAV value for the $M2$ octahedron is due to the fact that some of the O–$M2$–O angles within the $M2$ octahedron approach 90° with increasing cation disorder, while others deviate farther away from 90°. For example, while the O1–$M2$–O3 angle decreases from 84.93(4)° in P600 to 81.31(5)° in P1400, the O3–$M2$–O3 angle changes from 76.89(4) to 79.04(4)°.

In the $MgTi_2O_5$ structure, because the vector of the O3–O3 distance is parallel to the b axis, its significant reduction thus accounts largely for the observed shortening of the b dimension from P600 to P1400. The variation of the a and c dimensions with increasing cation disorder can be explained by the increase in size of the $M2$ octahedra, which form continuous edge-shared octahedral layers parallel to the a–c plane. The net result of the different behavior of a, b, and c as a function of cation disorder is the increase in the unit-cell volume for more disordered samples. Structurally, the greater unit-cell volume for the more disordered sample results from the less efficient packing of cation polyhedra, owing to the fact that larger Mg atoms occupy the smaller $M2$ octahedra. Similar phenomena have been found in many other minerals with edge-sharing octahedral sites (18). In other words, the ordered structure provides a more efficient packing arrangement of $M1$ and $M2$ in $MgTi_2O_5$, which, according to Hazen and Navrotsky (18), may be favored by the high-pressure environments.

Another noticeable change due to cation disordering is straightening of the bands consisting of the $M1$ and $M2$ octahedra. The kinking of the bands of the $M1$ and $M2$ octahedra can be described by the O3–O1–O3′ and O1–O3–O3′ angles (Fig. 1). These two angles, both of which vary linearly with the disorder parameter, straighten by 6.2° and 3.1°, respectively, from P600 to P1400 (Table 4). The unkinking of the bands of the $M1$ and $M2$ octahedra stems principally from the considerable shortening of the O3–O3′ distance within the $M1$ octahedron and the O2–O3 edge shared by $M1$ and $M2$.

A close correlation exists between magnitudes of atomic isotropic displacement factors (B_{iso}) and the disorder parameter: with increasing cation disorder, B_{iso} values of all atoms increase (Table 2). The apparent thermal motion of $M1$ probably results from atomic statically positional disorder, rather than thermal vibration. This conclusion is supported by the change in the anisotropy of the $M1$ displacement ellipsoid: while the degree of distortion for the $M1$ octahedron decreases significantly from P600 to P1400, the anisotropy of the $M1$ displacement ellipsoid, defined as $(r_3 - r_1)/0.5(r_3 + r_1)$, increases from 0.02 to 0.05, where r_3 and r_1 are the longest and shortest ellipsoidal axes, respectively. Relative to $M1$ and $M2$, the B_{iso} factors of oxygen atoms show much stronger dependence on the cation distribution. From P600 to P1400, the average B_{iso} value of three oxygen atoms (O1, O2, and O3) increases by $\sim$46%, whereas that of two cations increases by $\sim$24%. Of all oxygen atoms, the B_{iso} factor of O1 increases most ($\sim$60%) and that of O2 least ($\sim$34%). The largest increase in the B_{iso} value of O1 may be in part correlated with the straightening of the O3–O1–O3′ angle, since O1 acts as a pivot point for the stretching of the octahedral bands. Similar to $M1$, the relatively large B_{iso} value of O1 in more disordered samples could be a reflection of the increase in the atomic positional disorder at the O1 site. Yet, the O1 apparent thermal motion may also be in part a real representation of atomic thermal vibration as a consequence of compensation for an electron density distribution related to a local charge imbalance on O1. In the $MgTi_2O_5$ structure,

both O2 and O3 have bond valences close to the ideal value (2.0 v.u.), whereas O1 is underbonded. Calculated based on the method of Brown (21), the charge imbalance of O1 is -0.124 in P600, but is slightly increased to -0.176 in P1400. An ongoing study on the $MgTi_2O_5$ structure at high pressures may provide us with insights into the cause for the larger B_{iso} factors in more disordered samples, because pressure has little influence on atomic B_{iso} factors that principally represent thermal vibration (22), but it could reduce B_{iso} factors that result predominately from statically positional disorder (23). Regardless of the nature of the apparent thermal motions for atoms in the $MgTi_2O_5$ structure, the large atomic B_{iso} factors in more disordered samples may render evidence for possible changes in lattice vibrations with increasing cation disorder. Such changes have been argued by Brown and Navrotsky (12) to be responsible for the observed nonzero value of the nonconfigurational entropy of disordering in $MgTi_2O_5$. Further vibrational spectroscopy study on $MgTi_2O_5$ with different ordering states may provide us with information necessary to explain the changes in vibrational heat capacity.

ACKNOWLEDGMENTS

We thank N. Boctor for his kind help in the synthesis and quenching experiments with the $MgTi_2O_5$ crystals. X-ray diffraction work and a postdoctoral fellowship to H.Y. at the Geophysical Laboratory are supported by NSF Grant EAR-9218845, the Center for High Pressure Research, and the Carnegie Institution of Washington.

REFERENCES

1. G. Bayer, *J. Less-Common Met.* **24,** 129 (1971).
2. A. Navrotsky, *Am. Mineral.* **60,** 249 (1975).
3. B. A. Wechsler, *Am. Mineral.* **62,** 913 (1977).
4. B. A. Wechsler and A. Navrotsky, *J. Solid State Chem.* **55,** 165 (1984).
5. B. A. Wechsler and R. B. Von Dreele, *Acta Crystallogr. B* **45,** 542 (1989).
6. R. M. Hazen and H. Yang, *Science* **277,** 1965 (1997).
7. M. D. Lind and R. M. Housley, *Science* **175,** 521 (1972).
8. J. R. Smyth, *Earth Planet. Sci. Lett.* **24,** 262 (1974).
9. D. Virgo and F. E. Huggins, *Carnegie Inst. Wash. Year Book* **74,** 585 (1975).
10. B. A. Wechsler, C. T. Prewitt, and J. J. Papike, *Earth Planet. Sci. Lett.* **29,** 91 (1976).
11. M. F. Brigatti, S. Contini, S. Capedri, and L. Poppi, *Eur. J. Mineral.* **5,** 73 (1993).
12. N. E. Brown and A. Navrotsky, *Am. Mineral.* **74,** 902 (1989).
13. H. E. King and L. W. Finger, *J. Appl. Crystallogr.* **12,** 374 (1979).
14. M. S. Lehmann and F. K. Larsen, *Acta Crystallogr. A* **30,** 580 (1974).
15. L. W. Finger and E. Prince, Nat. Bur. of Stand. Technol. Note 854, 1975.
16. J. A. Ibers and W. C. Hamilton, "International Tables for X-ray Crystallography," Vol. IV, Kynoch, Birmingham, 1974.
17. P. J. Becker and P. Coppens, *Acta Crystallogr. A* **31,** 417 (1975).
18. R. M. Hazen and A. Navrotsky, *Am. Mineral.* **81,** 1021 (1996).
19. K. Robinson, G. V. Gibbs, and P. H. Ribbe, *Science* **172,** 567 (1971).
20. R. D. Shannon and C. T. Prewitt, *Acta Crystallogr. B* **25,** 925 (1969).
21. I. D. Brown, *in* "Structure and Bonding in Crystals" (M. O'Keefe and A. Navrotsky, Eds.), Vol. 2, Academic Press, New York, 1981.
22. L. W. Finger and H. E. King, *Am. Mineral.* **63,** 337 (1978).
23. H. Yang, R. M. Hazen, R. T. Downs, and L. W. Finger, *Phys. Chem. Minerals* **24,** 510 (1997).